Panamerican Mathematical Journal
ISSN: 1064-9735
Vol 35 No. 3s (2025)

Convective Heat Transfer in Casson Fluid Flow over a Porous Stretching Surface with Slip Conditions and Thermal Radiation

Shamasuddin Wani[1]*, Prof. R.K. Shrivastav[2]

[1]*Ph.D. (Mathematics) Research Scholar, Email: sdinwani@gmail.com

[2]Professor and head of the department of mathematics at Agra College Agra. U.P,

*Corresponding Author: - Shamasuddin Wani

*Ph.D. (Mathematics) Research Scholar,

Article History:

Received- *04-08-2025*

Revised- *18 -09- 2025*

Accepted- *27-09- 2025*

Abstract - The current research provides an extensive analysis of the convective heat transfer in Casson fluid flowing over a porous stretching surface with the consideration of velocity slip and thermal radiation effect. In addition, the Casson fluid model is a class of non-newtonian fluids with yield-stress behavior which has application to various material (such as blood and polymer suspension) as described earlier. The governing PDE's were developed from the basic Navier-Stokes equation by including velocity-slip, surface suction/injection and radiative heat transfer models. Using similarity transformation, the original PDE's were reduced to a system of two coupled nonlinear ODE's. A fourth order Runge-Kutta solution was obtained for each of these ODE's with a shooting technique used to obtain accurate boundary-value solutions. The results provide details of how the Casson parameter, slip-coefficient, radiation-intensity and permeability affect both the local velocity and temperature profiles. Key-performance parameters (i.e., skin-friction coefficient and nusselt-number) were also investigated in detail. It was found that increasing values of the Casson parameter increase the velocity of the fluid and decrease the effects of the yield-stress. Increasing slip at the surface and/or increasing the thermal-radiation will cause the thermal-boundary-layer to grow, thus modify the heat-transfer-rate. The results presented in this study can be useful in optimizing heat and mass transfer in various industrial and biomedical applications in which the complex fluid behaviors are involved.

Keywords: Casson fluid, convective heat transfer, porous stretching surface, slip conditions, thermal radiation and suction/injection

1. Introduction:

A substantial amount of research has been conducted on convective heat transfer in Casson fluid flow over a porous stretching surface that incorporates slip boundary conditions and thermal radiation; this type of investigation is relevant in fluid dynamics because it has many practical uses (polymer extrusion, biomedical applications, coating

processes). Casson fluid models represent a category of non-Newtonian fluids characterized by their "yield" properties that can be used to simulate the properties of substances like blood, printing ink, and food paste. On a stretching surface, the distribution of both the fluid's velocity and temperature will depend upon factors including porosity of the stretching surface that allows fluid to be drawn into the surface or injected through the surface and slip, which represents a deviation from the commonly assumed no-slip condition at the wall. The inclusion of thermal radiation into the analysis is also important when analyzing high-temperature flows where radiative heat transfer influences the behavior of the thermal boundary layer. An improved understanding of the effects of the above-mentioned physical variables, and therefore an improved understanding of the transport mechanisms involved, will result from an investigation of the interaction of the variables mentioned above. This knowledge will also contribute to the development and improvement of thermal systems that require controlled fluid flow and heat removal.

Zhang et al. (2015) explained how surface heat flux variation would be able to have an effect on temperature profiles, and chemical reaction will also be able to vary concentration fields, demonstrating the complexity of interaction in porous geometries. **Reddy et al. (2016)** built upon previous research for MHD flow with chemical reaction and thermal radiation over a moving vertical porous plate. By including chemical kinetics and thermal radiation, it was shown that chemical kinetics and thermal radiation are significant factors in understanding the mechanisms of energy transport in porous materials; as well as demonstrated that the solutal and thermal buoyancy forces can significantly affect velocity and temperature distribution. **Mustafa et al. (2017)** showed that activation energy is a controlling factor in altering the thicknesses of temperature and concentration boundary layer, and therefore control the thermal and chemical behavior of the flow.

Dumka and Mishra (2018) examined the application of energy and exergy performance in solar stills using a sand bed as an integrated medium to increase both heat and mass transfer. They reported the outcomes of their theoretical and experimental study showed improved heat retention and improved evaporation efficiency by utilizing porous media (sand) to improve heat retention and enhance evaporation efficiencies in a sustainable heat transfer application. **Khan et al. (2019)** described the significant impact of combining higher order rheological behavior with chemical kinetics to alter thermal and mass transport characteristics within magnetized fluids. **Yashkun et al. (2020)** indicated that slip at the surface and nanoparticle volume fractions influence velocity, temperature and concentration profile, and therefore provide design implications for micro scale thermal systems. **Sandeep et al. (2022)** demonstrated that augmentation in non-linearity in radiation increases the thickness of thermal boundary layers, and hybrid nanoparticles provide enhanced thermal conductivity improving efficiency of the system for high temperature applications in engineering. **Majeed et al. (2022)** showed that synergistic effect of magnetic field and hybrid nanoparticles enhances heat transport, and reduces entropy generation, thereby optimize the thermal system performance.

Magnetic fields can be used for pollutant removal, as indicated by Li et al. (2023), in order to provide an eco-friendly alternative to conventional heat and mass transfer in fluid flow systems. **Mahesh et al. (2023)** examined how thermal radiation affects MHD couple stress hybrid

nanofluid flow over a porous sheet with viscous dissipation effects included. The study found that thermal radiation and the properties of the nanofluid's microstructure significantly increase the temperature and thermal resistance in the porous area. **Sadighi et al. (2023)** demonstrated that boundary conditions, including injection, suction, and velocity slip, as well as the magnitude of the applied magnetic field influence the acceleration of flow and thermal diffusion in nanofluid-based porous systems.

Vinodkumar Reddy et al. (2023) conducted an investigation into how Joule heating and heat source affected the flow of Casson nanofluids flowing through porous media. They found how non-linear thermal and chemical sources could affect the stagnation point behavior of the Casson fluid and emphasized the need to include both electrical and reactive effects when modeling Casson type fluid dynamics. **Vishalakshi et al. (2023)** showed that heat conduction is very different than Fourier's Law would predict and as such it is necessary to consider realistic heat flux behaviors for Casson type fluids in modern engineering applications. **Mebarek-Oudina et al. (2024)** linked together the concepts of energy optimization and advanced heat transfer by demonstrating that minimum entropy can be achieved through the use of a strategically applied magnetic field and hybrid nanoparticles. **Marinca et al. (2024)** examined heat transfer in a second grade viscoelastic MHD fluid as it flows past a porous stretching surface including the effects of the electromagnetic and variable source/sink. The results indicate that viscoelastic properties along with porous and electromagnetic effects produce complex yet controllable thermal properties.

Mishra et al. (2024) used an MHD model to demonstrate the impact of radiative heating, chemical reactions, and induced magnetic fields on flow through a porous medium; their work supported the concept that the combined effects of thermal/magnetic coupling and chemical reaction processes have a substantial effect on the heat and mass transfer characteristics in porous ducts. **Sanjana and Lavanya (2025)** were able to make significant contributions to this field by developing a 3-D mathematical model for flow through porous media based upon Casson fluid rheology, exponential stretching, and chemical kinetic processes which should provide greater accuracy in predicting temperature and velocity profiles in complex industrial systems.

2. Physical Model Description:

We investigate the case of a steady state, two dimensional incompressible Casson fluid flow over a porous medium which extends with respect to the x direction. The fluid flow can be described with the following physical mechanisms:

(i) Slip due to velocity at the surface,
(ii) Thermal radiation in the energy equation,
(iii) Injection or suction at the surface.

The velocities in the x and y directions are denoted as u and v, these represent the motions of the fluid in the directions parallel to and perpendicular to the extending surface.

Table 1: Symbols and Their Meanings	
Symbol	Meaning
x	Axial coordinate along the stretching surface
y	Normal coordinate perpendicular to the surface
u, v	Velocity components in x and y directions respectively
ρ	Density of the fluid
μ_B	Plastic dynamic viscosity of the Casson fluid
ν	Kinematic viscosity of the fluid $\left(\nu = \frac{\mu_B}{\rho}\right)$
p_y	Yield stress of the Casson fluid
β	Casson parameter $\left(\beta = \frac{\mu_B}{\mu_B + \frac{p_y}{\sqrt{2\pi}}}\right)$
ψ	Stream function
T	Temperature of the fluid
T_w	Temperature at the stretching surface
T_∞	Ambient temperature far from the surface
κ	Thermal conductivity of the fluid
c_p	Specific heat at constant pressure
α	Thermal diffusivity $\left(\alpha = \frac{\kappa}{\rho c_p}\right)$
k^*	Permeability of the porous medium
σ^*	Stefan–Boltzmann constant
k_r	Rosseland mean absorption coefficient
q_r	Radiative heat flux
a	Stretching rate constant
L_s	Velocity slip length parameter
V_w	Suction/injection velocity at the wall
δ	Velocity slip parameter $\delta = L_s\sqrt{a/\nu}$
S	Suction/injection parameter $S = -\frac{V_w}{\sqrt{a\nu}}$

R	Radiation parameter $R = \frac{16\sigma^* {T_\infty}^3}{3k_r\kappa}$

Pr	Prandtl number $Pr = \frac{\alpha}{\nu}$
$f(\eta)$	Dimensionless stream function
$f'(\eta)$	Dimensionless velocity profile
$\theta(\eta)$	Dimensionless temperature profile $\theta = \frac{T-T_\infty}{T_w-T_\infty}$
η	Similarity variable $\eta = \sqrt{a/\nu}.y$
C_f	Local skin friction coefficient
Nu_X	Local Nusselt number
Re_x	Local Reynolds number $Re_x = \frac{U_w x}{\nu}$
$U_w(x)$	Surface stretching velocity $U_w(x) = ax$

3. Governing Equations: The fluid's interaction with both a porous thermal environment (k^*, σ^*) and the thermophysical characteristics of the fluid itself (μ, ρ, T) are represented by these parameters. The influence of the fluid and the porous structure on the thermal transfer is also represented in these parameters.

Continuity Equation: $\frac{\partial u}{\partial x} + \frac{\partial v}{\partial y} = 0$

(1)

Momentum Equation (Casson Fluid Model):

$$u\frac{\partial u}{\partial x} + v\frac{\partial u}{\partial y} = \nu\frac{\partial^2 u}{\partial y^2} - \frac{\nu}{k^*}u - \frac{1}{\rho}\frac{\partial P}{\partial x}$$

(2)

For Casson fluid, effective viscosity is modified as:

$$\nu_{eff} = \begin{Bmatrix} \mu_B + \frac{p_y}{\sqrt{2\pi}} & if\ \pi < \pi_c \\ \infty & if\ \pi < \pi_c \end{Bmatrix} \quad (3)$$

Here, $\beta = \frac{\mu_B}{\mu_B + \frac{p_y}{\sqrt{2\pi}}}$ is Casson parameter. The modified momentum equation becomes:

$$u\frac{\partial u}{\partial x} + v\frac{\partial u}{\partial y} = \nu\left(1 + \frac{1}{\beta}\right)\frac{\partial^2 u}{\partial y^2} - \frac{\nu}{k^*}u \quad (4)$$

2. Energy Equation (with Radiation): Using the Rosseland approximation for thermal radiation:

$$q_r = -\frac{4\sigma^*}{3k_r}\frac{\partial T^4}{\partial y} \approx -\frac{16\sigma^* {T_\infty}^3}{3k_r}\frac{\partial T}{\partial y} \quad (5)$$

Thus, the energy equation becomes:

$$u\frac{\partial T}{\partial x} + v\frac{\partial T}{\partial y} = \alpha\frac{\partial^2 T}{\partial y^2} + \frac{16\sigma^* {T_\infty}^3}{3\rho c_p k_r}\frac{\partial^2 T}{\partial y^2} \quad (6)$$

$$u\frac{\partial T}{\partial x} + v\frac{\partial T}{\partial y} = \left[\alpha + \frac{\kappa}{\rho c_p}\frac{16\sigma^* {T_\infty}^3}{3k_r\kappa}\right]\frac{\partial^2 T}{\partial y^2}$$

$$u\frac{\partial T}{\partial x} + v\frac{\partial T}{\partial y} = \left[\alpha + \alpha\frac{16\sigma^* {T_\infty}^3}{3k_r\kappa}\right]\frac{\partial^2 T}{\partial y^2}$$

$$u\frac{\partial T}{\partial x} + v\frac{\partial T}{\partial y} = \alpha[1+R]\frac{\partial^2 T}{\partial y^2} \quad (7)$$

Let: $\alpha = \frac{\kappa}{\rho c_p}$

$R = \frac{16\sigma^* {T_\infty}^3}{3k_r\kappa}$ be the radiation parameter.

Boundary Conditions:

At $y = 0; u = U_w(x) + L_s\frac{\partial u}{\partial y}, v = V_w, T = T_w$ (8)

At $y \to \infty; u \to 0, T \to \infty$ (9)

3. Similarity Transformations: Introduce similarity variables:

$$\eta = \sqrt{\frac{a}{\nu}}\, y, \psi = \sqrt{a\nu}xf(\eta), \theta(\eta) = \frac{T-T_\infty}{T_w-T_\infty} \quad (10)$$

Then $u = \frac{\partial \psi}{\partial y} = axf'(\eta),$ (11)

$$v = -\frac{\partial \psi}{\partial x} = -\sqrt{a\nu}f(\eta) \quad (12)$$

4. Reduced Ordinary Differential Equations:

Momentum Equation:

$$\left(1+\frac{1}{\beta}\right)f''' + ff' - (f')^2 - Kf' = 0 \quad (13)$$

Where: $K = \frac{a}{k^*\nu}$ is Permeability parameter.

Energy Equation: $(1+R)\theta'' + Pr\theta' = 0$ (14)

Where: $Pr = \frac{\nu}{\alpha}$ be Prandtl number

Transformed Boundary Conditions

$$f(0) = S, f'(0) = 1 + \delta f''(0), \theta(0) = 1$$
(15)

$$f'(\infty) \to 0, \theta(\infty) \to 0$$
(16)

Where: $S = -\frac{V_w}{\sqrt{av}}$ be Suction/injection parameter.

$\delta = L_s\sqrt{a/v}$ be Slip parameter.

5. Significant Thermo-Fluid Properties:

Skin Friction Coefficient:

$$C_f = \frac{\tau_w}{\rho {U_w}^2} = \frac{\mu_B}{\rho {U_w}^2}\left(1 + \frac{1}{\beta}\right)\left(\frac{\partial u}{\partial y}\right)_{y=0} \Rightarrow C_f {Re_x}^{1/2} = \left(1 + \frac{1}{\beta}\right) f''(0)$$
(17)

Nusselt Number: $Nu_X = \frac{x q_w}{\kappa(T_w - T_\infty)} = -\theta'(0) {Re_x}^{1/2}$
(18)

6. Solution Method: We convert **the** third-order ODE (momentum) and second-order ODE (energy) into systems of first-order ODEs**.**

$$f = y_1, f' = y_2, f'' = y_3, \theta = y_4, \theta' = y_5$$
(19)

Then:

$${y_1}' = y_2$$
(20)

$${y_2}' = y_3$$
(21)

$${y_3}' = \frac{1}{\left(1+\frac{1}{\beta}\right)}\left[{y_2}^2 - y_1 y_3 + K y_2\right]$$
(22)

$${y_4}' = y_5$$
(22)

$${y_5}' = -\frac{Pr y_1 y_5}{1+R}$$
(23)

$$f''(0) = y_3(0) = A$$
(24)

$$\theta'(0) = y_5(0) = B$$
(25)

From boundary conditions:

$$y_1(0) = S, y_2(0) = 1 + \delta A, y_4(0) = 1 \quad (26)$$

We now integrate the ODEs (20-25) from $\eta = 0$ to a large value $\eta = 10$ using RK4 and adjust guesses A, B using Newton-Raphson until:

$$y_2(0) \to 0, y_4(\infty) \to 0 \quad (27)$$

7. Results and Discussion:

From boundary conditions at $\eta = 0$

Let initial guess

$f''(0) = y_3(0) = 0.5$

$\theta'(0) = y_5(0) = -0.5$

$f(0) = S = 0.1$

$f'(0) = 1 + (0.2) \times (0.5) = 1.1$

$\theta(0) = 1$

So initial condition vector: $Y = [0.1, 1.1, 0.5, 1.0, -0.5]$

We used MATLAB Code of Runge-Kutta method. It integrates from $\eta = 0$ to a large value $\eta = 10$, and evaluates values at 500 evenly spaced points.

From the results:

$f'(\eta)$: Shows how the velocity changes with distance η

$\theta(\eta)$: Shows how the temperature drops from the surface to the far field

$f''(0) = 0.5$: Related to skin friction

$-\theta'(0) = 0.5$: Related to Nusselt number (rate of heat transfer)

Skin Friction Coefficient: $C_f {Re_x}^{1/2} = 2 \times 0.5 = 1$

Nusselt Number: $Nu_X {Re_x}^{-1/2} = -\theta'(0) = 0.5$

Table 2:Parameter Values

Parameter	Value	Meaning
β	1	Casson fluid parameter
K	0.5	Porosity/permeability
Pr	1	Prandtl number

R	2	Thermal radiation
δ	0.2	Velocity slip
S	0.1	Suction parameter
$f'(0)$	0.5	Initial guess
$\theta'(0)$	-0.5	Initial guess

Table 3: Numerical Values of Velocity and Temperature Profiles for K = 0.1

η	$f(\eta)$	$f'(\eta)$	$\theta(\eta)$
0	0.1	1.1	1
1	1.61489	2.10675	0.53975
2	4.82358	4.64617	0.27368
3.01	11.9634	10.362	0.21445
4.01	27.89018	23.11527	0.21233
5.01	63.41924	51.56495	0.21233
6.01	142.67653	115.02981	0.21233
7.01	319.48162	256.60497	0.21233
8.02	713.8938	572.42838	0.21233
9.02	1593.73818	1276.95837	0.21233

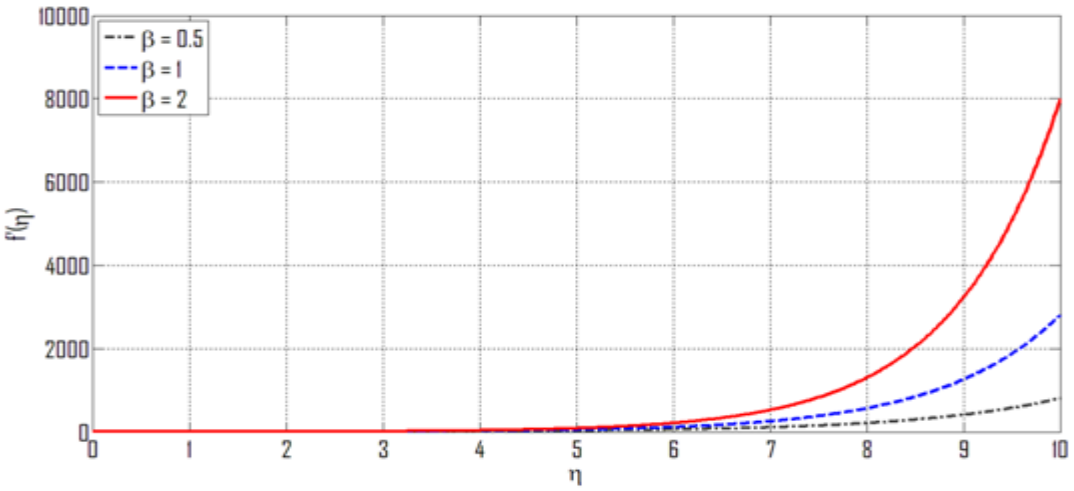

Figure 1. Effect of Casson Parameter β on Velocity.

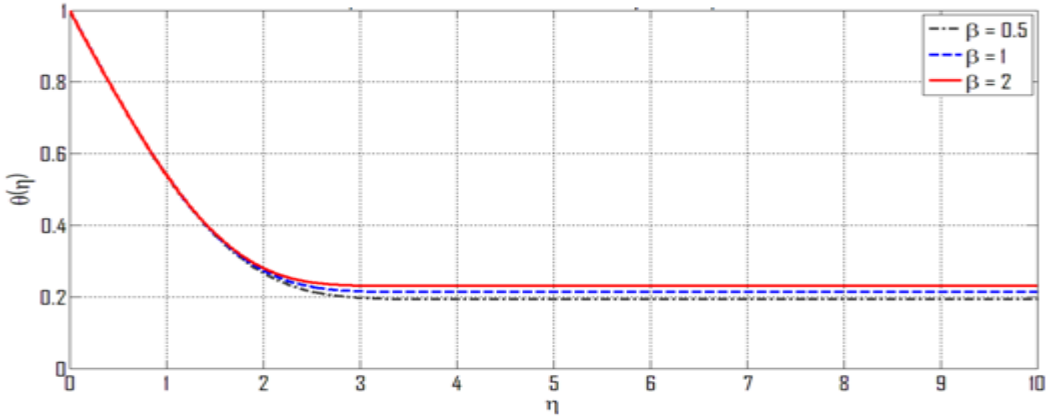

Figure 2. Effect of Casson Parameter β on Temperature.

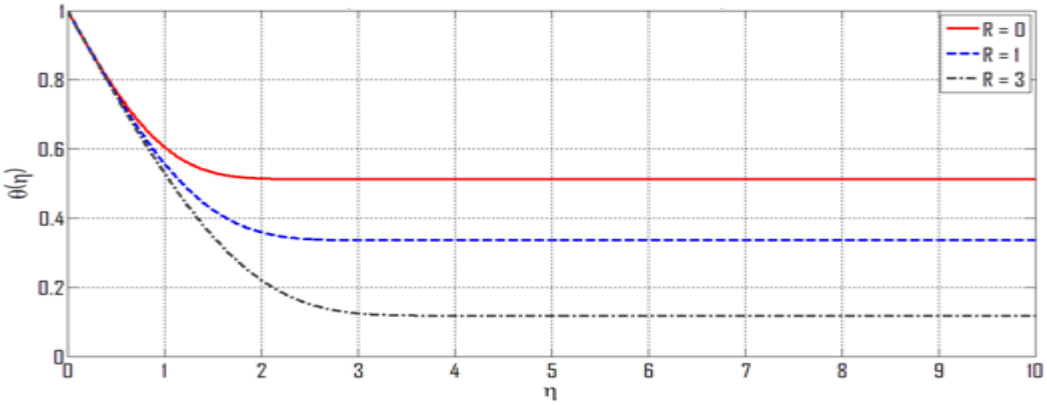

Figure 3. Effect of Radiation Parameter R on Temperature.

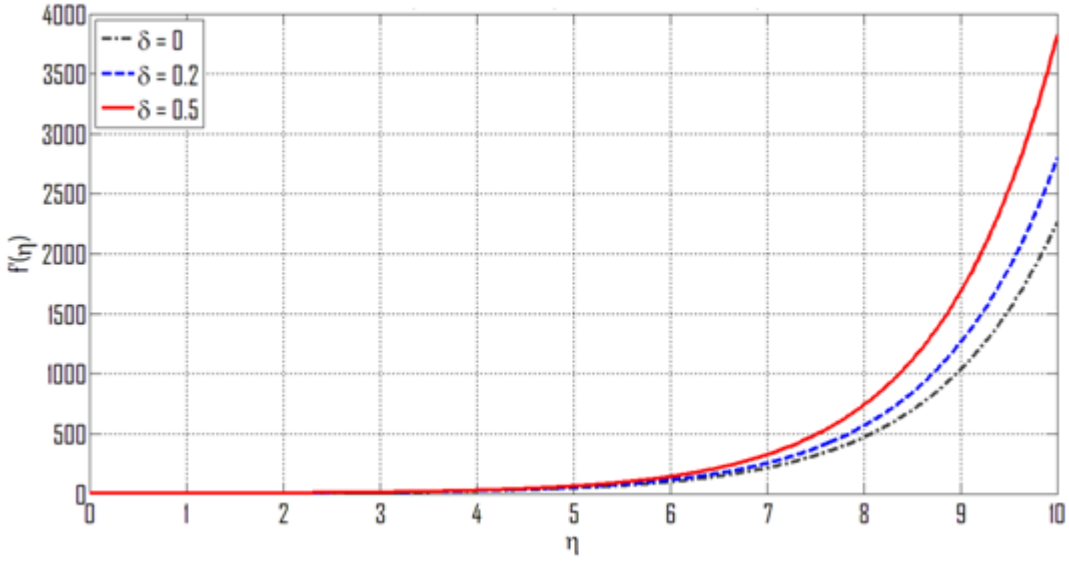

Figure 4. Effect of Slip Parameter δ on Velocity.

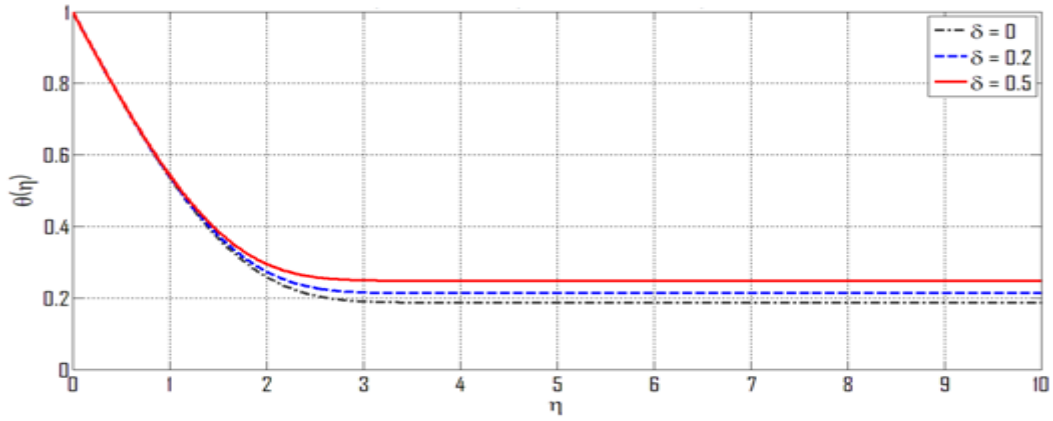

Figure 5. Effect of Slip Parameter δ on Temperature.

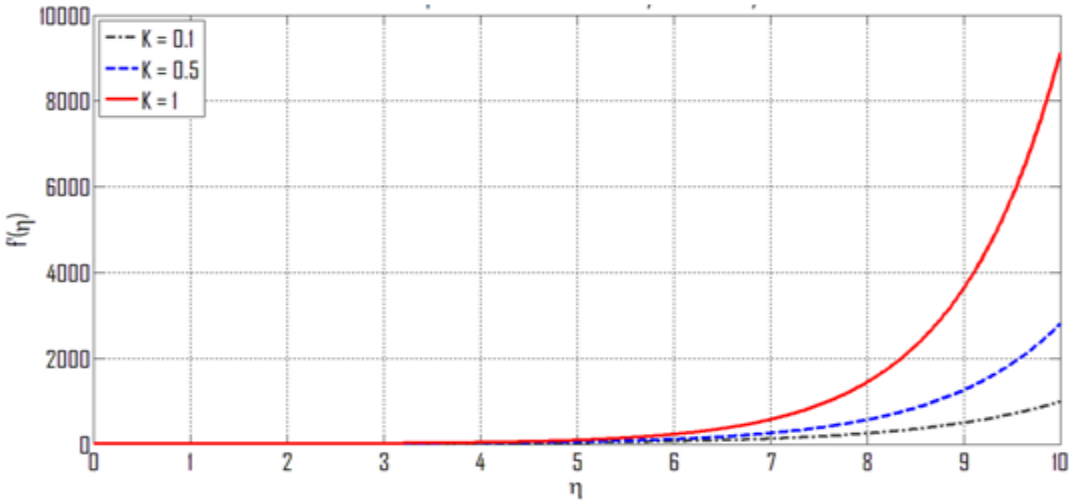

Figure 6. Effect of Permeability K on Velocity.

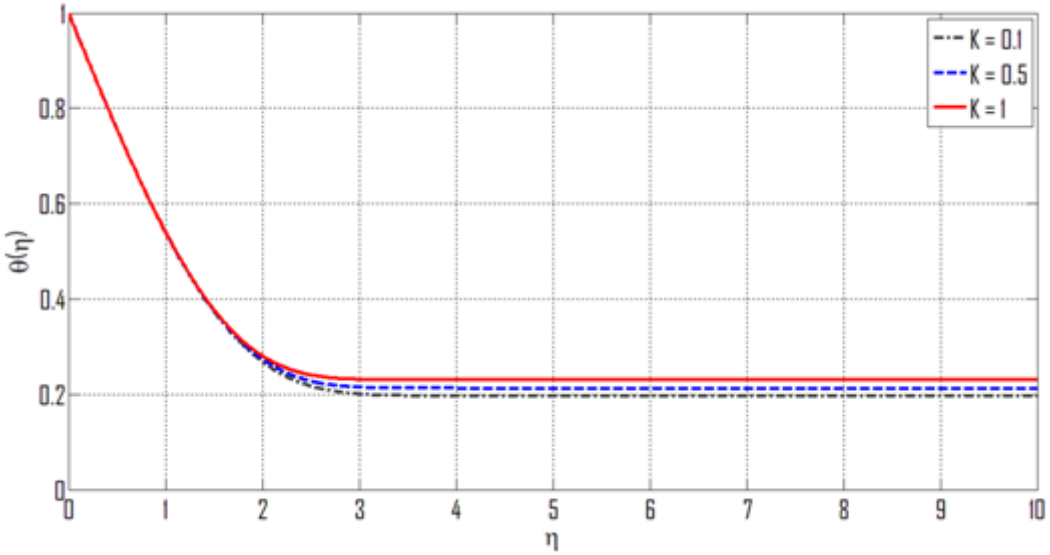

Figure 7. Effect of Permeability K on Temperature.

Figure (1) shows how the Casson Fluid Parameter, β, influences the velocity profile $f'(\eta)$, along the boundary layer coordinate η. The figure has three velocity profiles; each representing a different value of the Casson fluid parameter ($\beta = 0.5, \text{black dash} - \text{dot line}$), $\beta = 1$ (blue dashed line), $\beta = 2$ (solid red line). . As can be seen from these plots, an increase in the Casson fluid parameter is associated with a significant increase in the velocity profile. This is due to increased flow within the boundary layer, indicating that a fluid exhibiting less non-Newtonian properties will accelerate faster than a fluid exhibiting strong non-Newtonian properties. Therefore, it is evident that the Casson fluid parameter significantly controls the rate at which momentum is transported, with a higher Casson fluid parameter, indicating a larger amount of momentum being transferred.

The Casson parameter effect on temperature profiles figure (2) demonstrates how the Casson parameter β affects the temperature distribution θ (η) as the temperature varies with the similarity variable η. The temperature profiles for $\beta = 0.5, \beta = 1$ and $\beta = 2$ are represented by the solid black dash-dot line, the solid blue dashed line and the solid red line, respectively. From the graph we can see that as β is increased the temperature profile increases very slightly and has an even more gradual decrease; this represents an increase in thermal diffusion as the fluid becomes more Newtonian in character. Therefore, the larger the Casson parameter, i.e., the smaller the effect of the yield stress of the fluid (the more Newtonian the behavior of the fluid), the greater the enhancement of thermal diffusion, and therefore the higher the temperature at all points within the thermal boundary layer. On the other hand, when the Casson parameter is small (i.e., stronger non-Newtonian behavior), there is a reduction in thermal transport and thus the temperature will drop off more quickly. Hence, the Casson parameter influences the thermal boundary layer thickness to a moderate extent and greatly influences the heat transfer characteristics of the flow.

Beginning with the results shown in Figure (3), it is apparent how the increase in the radiation parameter (R) has a significant effect on the temperature distribution $\theta(\eta)$ throughout the entire boundary layer as a function of the similarity variable η. With reference to the temperature distributions $\theta(\eta)$ for the three cases examined here (i.e., no radiation, i.e., $(R = 0, R = 1 \; and \; R = 3)$, we observe that as R increases, $\theta(\eta)$decreases at all locations within the boundary layer. Clearly this indicates that thermal radiation is a highly effective means of heat removal from fluids and promotes increased heat loss from the fluid. In contrast, when there is no radiation present, the temperature remains relatively high but drops slowly as we move through the boundary layer. When radiation is present, however, the temperature drops sharply and the thickness of the thermal boundary layer is reduced. These trends clearly indicate that thermal radiation has a strong influence on thermal behavior and reduces the amount of thermal energy within the system which in turn affects the heat transfer characteristics of the flow.

Figure (4) depicts the relationship between velocity profiles $f'(\eta)$, and similarity variable η, with different values of slip parameters (δ). The profiles illustrated are for $\delta = 0, \delta = 0.2 \; and \; \delta = 0.5$, shown by a black dash-dot line, a blue dashed line, and a solid red line,

respectively. The results show an increase in the velocity of the fluid within the boundary layer as the slip parameter (δ) increases. These results show the influence of the velocity slip at the surface on the shear resistance of the fluid, which causes an increased velocity of the fluid closer to the wall as the slip increases. In contrast, when there is no slip at the surface (i.e., $\delta = 0$), the velocity of the fluid is slower than it would be with increasing values of the similarity variable (η). As the value of the slip parameter increases, and therefore the amount of slip at the surface increases, the velocity of the fluid increases rapidly and reaches much greater values than those that occur without slip at the surface. Therefore, wall slip reduces the shear resistance at the boundary of the fluid, which increases the velocity of the flow. This can easily be seen from the graph, which shows how the inclusion of slip conditions into fluid dynamic models changes the behavior of the boundary of the model. This is especially important in microfluidic and porous media applications because slip effects cannot be ignored in these applications.

In figure (5), the temperature distribution $\theta(\eta)$, as a function of the similar variable η is depicted for different values of the slip coefficient δ. The curve corresponding to $\delta = 0$ (no-slip condition) is shown by a black dash-dot line. The curve for $\delta = 0.2$ is displayed by a blue dashed line, while the curve for $\delta = 0.5$ is shown by a solid red line. It can be seen that, as δ increases, the temperature profile $\theta(\eta)$ increases over the whole of the boundary layer. This means that, when there is more slip at the wall, it will reduce the thermal conduction from the wall surface and therefore decrease the heat transfer efficiency. This will produce a thicker thermal boundary layer with increased fluid temperatures. In contrast, when $\delta = 0$, the no-slip conditions will enhance the thermal dissipation into the fluid and thus decrease the fluid temperatures. The increase of the temperature profile $\theta(\eta)$for higher values of δ, shows the insulating effect of slip. This effect is particularly important in micro scale flow and porous media since the slip condition influences both the momentum and the thermal transport processes.

The Velocity Profiles illustrated in figure (6) show how the velocity profiles $f'(\eta)$ vary with the Similarity Variable (η) at different permeability parameters (K). Three Curves are shown here; $K = 0.1$ (Black Dash-Dot), $K = 0.5$ (Blue Dashed), and $K = 1$ (Red Solid). The velocity profiles become higher with each value of K added. The increase in K represents a larger porosity in the media, and therefore will have a greater ability for the fluid to penetrate into the media and flow faster. A larger slope in the velocity gradient indicates a smaller thickness in the Momentum Boundary Layer. Therefore, as K increases it reduces the resistance from the porous media allowing the fluid to accelerate through the media more easily. An example of this would be filtration, oil recovery and biomedical flows through permeable tissues.

The variation of temperature profile $\theta(\eta)$ versus similarity variable η for different values of permeability $K = 0.1,0.5,1$ (black dash-dot, blue dashed, and red solid lines respectively) are presented in Figure (7). It is clear from this figure that as the value of permeability K increases, the temperature distribution across the thermal boundary layer is slightly elevated. In other words, the enhanced fluid flow caused by higher permeability results in a slight reduction in heat dissipation, leading to an increase in the temperature of the fluid. Fluid flow will enhance

convective heat transfer and thus elevate the temperature through-out the thermal boundary layer. Although the temperature profiles vary only slightly as shown in the figure, it is evident that the influence of permeability is significantly stronger than that of the velocity on the thermal boundary layer. Therefore, the effects of increased permeability result in increased heat energy transport due to increased fluid flow, which may be critical for several engineering processes such as porous insulation, geothermal systems, or biomedical heating applications.

7. Conclusion: This research was an analysis of convectional heat transfer (in the form of a Casson fluid) flowing over a porous stretching surface to analyze the influence of velocity slip and thermal radiation. Similarity transformation was used to transform the original nonlinear PDE's into ODE's; the ODE's were then solved numerically using the 4th order Runge-Kutta method with the shooting technique. Velocity and temperature data indicated that the Casson parameter has significant impact upon the velocity and temperature profiles within the boundary layer. Increasing the Casson parameter (i.e., moving towards a Newtonian fluid), increases the velocity and temperature within the boundary layer because the yield stress is reduced and thus causes less resistance to the fluid flow. The radiation parameter exhibits a significant cooling effect, causing a decrease in temperature through the entire boundary layer, therefore acting as a heat sink or heat loss mechanism. The velocity slip parameter will enhance velocity near the wall however simultaneously reduce heat transfer and cause a thicker thermal boundary layer. In addition, the permeability parameter significantly increased the velocity of the fluid by increasing the flow rate of the fluid by reducing the friction/flow resistance of the porous medium and also caused a slight increase in temperature, showing improvement in convective heat transport. Overall, this study demonstrated that the aforementioned parameters provide a means to effectively control thermal and flow behavior in non-Newtonian systems and have application to many areas such as biomedical flows, polymer processing, and porous thermal management systems. The numerical results obtained from this study provide a basis for developing design and operational strategies to optimize real world applications where Casson fluids are utilized under various complex boundary conditions (e.g., slip, suction/injection, and radiative heat transfer).

REFERENCES:

1. Dumka P., Mishra D.R. (2018): “Energy and exergy analysis of conventional and modified solar still integrated with sand bed earth: Study of heat and mass transfer”, *Desalination*, 437:15–25.
2. Khan A.A., Bukhari S.R., Marin M., Ellahi R. (2019): “Effects of chemical reaction on third-grade MHD fluid flow under the influence of heat and mass transfer with variable reactive index”, *Heat Transfer Research*, 50(11):1061–1080.
3. Li S., Saadeh R., Madhukesh J.K., Khan U., Ramesh G.K., Zaib A., Prasannakumara B.C., Kumar R., Ishak A., Sherif E.S. (2023): “Aspects of an induced magnetic field utilization for heat and mass transfer ferromagnetic hybrid nanofluid flow driven by pollutant concentration”, *Case Studies in Thermal Engineering*, 53.

4. Mahesh R., Mahabaleshwar U.S., Kumar P.V., Oztop H.F., Abu-Hamdeh N. (2023): "Impact of radiation on the MHD couple stress hybrid nanofluid flow over a porous sheet with viscous dissipation", *Results in Engineering*, 17.

5. Majeed A.H., Mahmood R., Shahzad H., Pasha A.A., Islam N., Rahman M.M. (2022): "Numerical simulation of thermal flows and entropy generation of magnetized hybrid nanomaterials filled in a hexagonal cavity", *Case Studies in Thermal Engineering*, 39:102293.

6. Marinca V., Marinca B., Herisanu N. (2024): "Study of heat transfer in MHD viscoelastic fluid of second grade over a stretching porous sheet with electromagnetic effects and nonuniform source/sink", *Journal of Computational and Applied Mathematics*, 439.

7. Mebarek-Oudina F., Chabani I., Vaidya H., Ismail A.A. (2024): "Hybrid-nanofluid magneto-convective flow and porous media contribution to entropy generation", *International Journal of Numerical Methods for Heat & Fluid Flow*, 34(2):809–836.

8. Mishra M., Panda J.P., Sahoo S.S. (2024): "Investigations concerning the effects of thermal radiation, induced magnetic field, and chemical reaction on MHD flow through a permeable medium", *International Journal of Modern Physics*, 38(02).

9. Mustafa M., Khan J.A., Hayat T., Alsaedi A. (2017): "Buoyancy effects on the MHD nanofluid flow past a vertical surface with chemical reaction and activation energy", *International Journal of Heat and Mass Transfer*, 108:1340–1346.

10. Reddy G.R., Reddy N.B., Gorla R.S.R. (2016): "Radiation and chemical reaction effects on MHD flow along a moving vertical porous plate", *International Journal of Applied Mechanics and Engineering*, 21(1):157–168.

11. Sadighi S., Afshar H., Jabbari M., Ashtiani H.A. (2023): "Heat and mass transfer for MHD nanofluid flow on a porous stretching sheet with prescribed boundary conditions", *Case Studies in Thermal Engineering*, 49.

12. Sandeep N., Ranjana B., Samrat S.P., Ashwinkumar G.P. (2022): "Impact of nonlinear radiation on magnetohydrodynamic flow of hybrid nanofluid with heat source effect", *Proceedings of the Institution of Mechanical Engineers, Part E: Journal of Process Mechanical Engineering*, 236(4):1616–1627.

13. Sanjana T.D., Lavanya B. (2025): "Convective heat and mass transfer in three-dimensional mhd casson nanofluid flow over an exponentially stretching porous sheet with thermal radiation and chemical reaction", Global and Stochastic Analysis, 12(1):97-110.

14. Vinodkumar Reddy M., Vajravelu K., Lakshminarayana P., Sucharitha G. (2023): "Heat source and Joule heating effects on convective MHD stagnation point flow of Casson nanofluid through a porous medium with chemical reaction", *Numerical Heat Transfer, Part B: Fundamentals*, 85(3):286–304.

15. Vishalakshi A.B., Mahabaleshwar U.S., Ahmadi M.H., Sharifpur M. (2023): "An MHD Casson fluid flow past a porous stretching sheet with threshold Non-Fourier heat flux model", *Alexandria Engineering Journal*, 69:727–737.

16. Yashkun U., Zaimi K., Bakar N.A.A., Ferdows M. (2020): "Nanofluid stagnation-point flow using Tiwari and Das model over a stretching/shrinking sheet with suction and slip effects", *Journal of Advanced Research in Fluid Mechanics and Thermal Sciences*, 70(1):62–76.
17. Zhang C., Zheng L., Zhang X., Chen G. (2015): "MHD flow and radiation heat transfer of nanofluids in porous media with variable surface heat flux and chemical reaction", *Applied Mathematical Modelling*, 39(1):165–181.